

Variability selected high-redshift quasars on SDSS Stripe 82

N. Palanque-Delabrouille¹, Ch. Yeche¹, A. D. Myers^{2,6}, P. Petitjean³, Nicholas P. Ross⁴, E. Sheldon⁵, E. Aubourg^{1,7}, T. Delubac¹, J.-M. Le Goff¹, I. Pâris³, J. Rich¹, K. S. Dawson⁹, D. P. Schneider¹⁰, B. E. Weaver⁸, and others...

¹ CEA, Centre de Saclay, Irfu/SPP, F-91191 Gif-sur-Yvette, France

² Department of Astronomy, University of Illinois at Urbana-Champaign, Urbana IL 61801, USA

³ Université Paris 6, Institut d'Astrophysique de Paris, CNRS UMR7095, 98bis Boulevard Arago, F-75014 Paris, France

⁴ Lawrence Berkeley National Lab, 1 Cyclotron Road, Berkeley, CA 94720, USA

⁵ Brookhaven National Laboratory, Bldg 510, Upton, NY 11973

⁶ Max-Planck-Institut für Astronomie, Königstuhl 17, D-69117 Heidelberg, Germany

⁷ APC, 10 rue Alice Domon et Léonie Duquet, F-75205 Paris Cedex 13, France

⁸ Center for Cosmology and Particle Physics, New York University, New York, NY 10003 USA

⁹ University of Utah, Dept. of Physics & Astronomy, 115 S 1400 E, Salt Lake City, UT 84112

¹⁰ Department of Astronomy and Astrophysics, The Pennsylvania State University, 525 Davey Laboratory, University Park, PA 16802

Received xx; accepted xx

ABSTRACT

The SDSS-III BOSS Quasar survey will attempt to observe $z > 2.15$ quasars at a density of at least 15 per square degree to yield the first measurement of the Baryon Acoustic Oscillations in the Ly- α forest. To reach this goal, we have developed a method to identify quasars based on their variability in the *ugriz* optical bands. The method has been applied to the selection of quasar targets in the SDSS region known as Stripe 82 (the Southern equatorial stripe), where numerous photometric observations are available over a 10-year baseline. This area was observed by BOSS during September and October 2010. Only 8% of the objects selected via variability are not quasars, while 90% of the previously identified high-redshift quasar population is recovered. The method allows for a significant increase in the $z > 2.15$ quasar density over previous *ugriz*-based strategies, achieving a density of 24.0 deg^{-2} on average down to $g \sim 22$ over the 220 deg^2 area of Stripe 82. We applied this method to simulated data from the Palomar Transient Factory and from Pan-STARRS, and showed that even with data that has sparser time sampling than what is available in Stripe 82, including variability in future quasar selection strategies would lead to increased target selection efficiency in the $z > 2.15$ redshift range. We also found that Broad Absorption Line quasars are preferentially present in a variability than in a color selection.

Key words. Quasars; variability

1. Introduction

Baryonic Acoustic Oscillations (BAO) and their imprint on the matter power spectrum were first observed in the distribution of galaxies (Cole et al., 2005; Eisenstein et al., 2005). They can also be studied by using the H I Lyman- α absorption signature of the matter density field along quasar lines of sight (White, 2003; McDonald & Eisenstein, 2007). A measurement sufficiently accurate to provide useful cosmological constraints requires the observation of at least 10^5 quasars, in the redshift range $2.2 < z < 3.5$, over at least 8000 deg^2 (Eisenstein et al., in prep.). This goal is one of the aims of the Baryon Oscillation Spectroscopic Survey (BOSS) project (Schlegel et al., 2009), part of the Sloan Digital Sky Survey-III¹ which is currently taking data. One of the challenges of this survey is to build a list of targets that contains a sufficient number of quasars in the required redshift range.

Quasars are traditionally selected photometrically, based on their colors in various bands (Schmidt & Green,

1983; Croom et al., 2001; Richards et al., 2004, 2009; Croom et al., 2009). While these methods achieve good completeness at low redshift ($z < 2$), they present serious drawbacks for the selection of quasars at redshifts above 2.2. In particular, as was shown in Fan (1999), quasars with $2.5 < z < 3.0$ tend to occupy the same region of optical color space as the much more numerous stellar population, causing the selection efficiency (or purity) to drop below $\sim 50\%$ in that region. The same confusion occurs again for $3.3 < z < 3.8$. This was recently confirmed by Worseck & Prochaska (2010) who have demonstrated that the SDSS standard quasar selection systematically misses quasars with redshifts in the range $3 < z < 3.5$.

The separation of stars and quasars in the redshift range of interest can be improved by using the variability of quasars in the optical. Light curves sampled every few days over several years were used by the MACHO collaboration (Geha et al., 2003) to identify 47 quasars behind the Magellanic Clouds. In a similar way, the OGLE project (Dobrzycki et al., 2003) has identified 5 quasars behind the Small Magellanic Cloud. Three seasons of obser-

¹ <http://www.sdss3.org>

vation on high galactic latitude fields were used by QUEST to search for variable sources. Nine previously unknown quasars (Rengstorf et al., 2004) were discovered.

More recently, significant progress in describing the evolution with time of quasar fluxes has been made possible by the multi-epoch data in the SDSS Stripe 82 (York et al., 2000). Using large sample of over 10,000 quasars, deVries et al. (2004) and MacLeod et al. (2008) have characterized quasar light curves with structure functions. Concentrating on SDSS Stripe 82 data, Schmidt et al. (2010) developed a technique for selecting quasars based on their variability. Recent works have shown that the optical variability of quasars could be related to a continuous time stochastic process driven by thermal fluctuations (Brandon et al., 2009) and modelled as a damped random walk (MacLeod et al., 2010a; Kozłowski et al., 2010). This resulted in a structure function that was used by MacLeod et al. (2010b) to separate quasars from other variable point sources. A variant, based on a statistical description of the variability in quasar light curves, was suggested by Butler & Bloom (2010) for the selection of quasars using time-series observations in a single passband.

In this paper, we present a method to select quasar candidates, inspired from the formalism developed by Schmidt et al. (2010). The method was adopted by the BOSS collaboration to choose the objects that were targeted, during September and October 2010, in Stripe 82. This region covers 220 deg² defined by equatorial coordinates $-43^\circ < \alpha_{J2000} < 45^\circ$ and $-1.25^\circ < \delta_{J2000} < 1.25^\circ$. It was previously imaged about once to three times a year from 2000 to 2005 (SDSS-I), then with an increased cadence of 10-20 times a year from 2005 to 2008 (SDSS-II) as part of the SDSS-II supernovae survey (Frieman et al., 2008). With a sampling of 53 epochs on average, over a time span of 5 to 10 years (Abazajian et al., 2009), the SDSS Stripe 82 data is ideal for testing a variability selection of quasars. For the first time, in September and October 2010, the observational strategy of BOSS rested entirely on variability for the final selection (after loose initial color cuts as explained below). In contrast, all target lists in BOSS had been obtained so far from the location of the objects in color-color diagrams, following various strategies — such as the kernel density estimation method (Richards et al., 2004) or a neural network approach (Yeche et al., 2010).

Section 2 presents the formalism used to describe the variability in quasar light curves and gives the performance of the chosen selection algorithm on two test samples, one of stars and the other of quasars. Section 3 explains how this tool was applied to select two sets of targets in Stripe 82, and presents the results obtained. An extrapolation of this method to the full 10,000 deg² observed by SDSS, made possible by adding data from the Palomar Transient Factory (Rau et al., 2009), or from Pan-STARRS², is presented in Section 4. We conclude in Section 5.

2. Variability selection algorithm

The main purpose of this study was to develop an algorithm to select quasars in Stripe 82 based on their variability, while rejecting as many stars as possible. Spectroscopically confirmed stars and quasars in Stripe 82 were used to compute two sets of discriminating variables. The first one, used

to distinguish variable objects from non-variable stars, consists in the χ^2 of the light curve with respect to the mean flux, in each of the five photometric bands. The second one, which helps discriminating quasars from variable stars, consists in parameters that describe the structure function.

2.1. Quasar and star samples

For the quasar training sample, we used a list of 13328 spectroscopically confirmed quasars obtained from the 2dF quasar catalog (2QZ; Croom et al., 2004), the 2dF-SDSS LRG and Quasar Survey (2SLAQ) (Croom et al., 2009), the SDSS-DR7 spectroscopic database (Abazajian et al., 2009), the SDSS-DR7 quasar catalog (Schneider et al., 2010) and the first year of BOSS observations. These quasars have redshifts in the range $0.05 \leq z \leq 5.0$ (cf. Fig 1) and g magnitudes in the range $18 \leq g \leq 22$ (Galactic extinction-corrected).

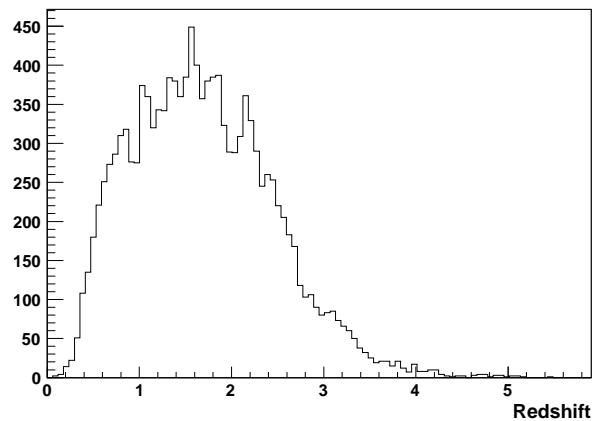


Fig. 1: Redshift distribution of the sample of quasars from all previous quasar surveys covering Stripe 82. This sample is used to test the variability algorithm and train its neural network.

For the star sample, we used 2697 objects observed by BOSS, initially tagged as potential quasars from color selection and spectroscopically confirmed as stars. Variability and color-selection are not fully independent: bright objects that are easily discarded by their colors are also easier to discard by their variability. Therefore, the use of these spectroscopically confirmed stars constitutes a conservative approach and corresponds exactly to the type of objects that we want to reject with the variability algorithm.

Light curves were constructed for these two samples from the data collected by SDSS. The collaboration used the dedicated Sloan Foundation 2.5 m telescope (Gunn et al., 2006). A mosaic CCD camera (Gunn et al., 1998) imaged the sky in five *ugriz* bandpasses (Fukugita et al., 1996). The imaging data were processed through a series of pipelines (Stoughton et al., 2002) which performed astrometric calibration, photometric reduction and photometric calibration. Typical examples of stellar and quasar light curves are shown in Figs. 2 and 3 respectively. The increased cadence after MJD 53500 are the SDSS-II supernovae search observations.

² <http://pan-starrs.ifa.hawaii.edu/public/home.html>

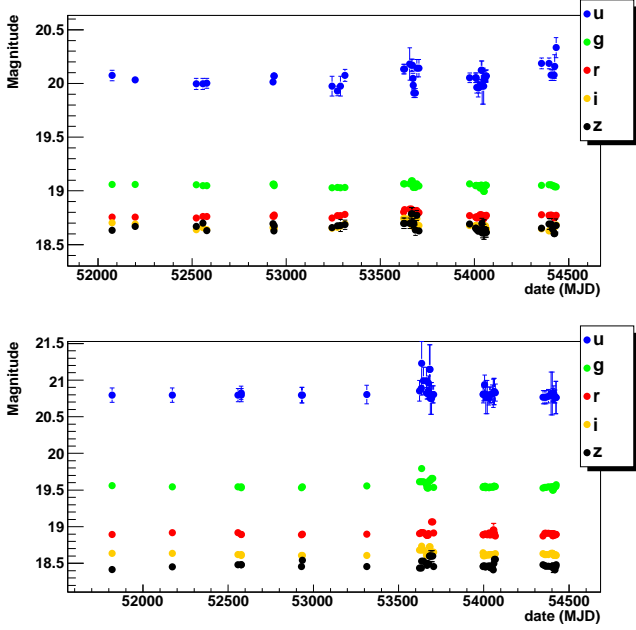


Fig. 2: Examples of light curves in the five SDSS photometric bands for stars in Stripe 82.

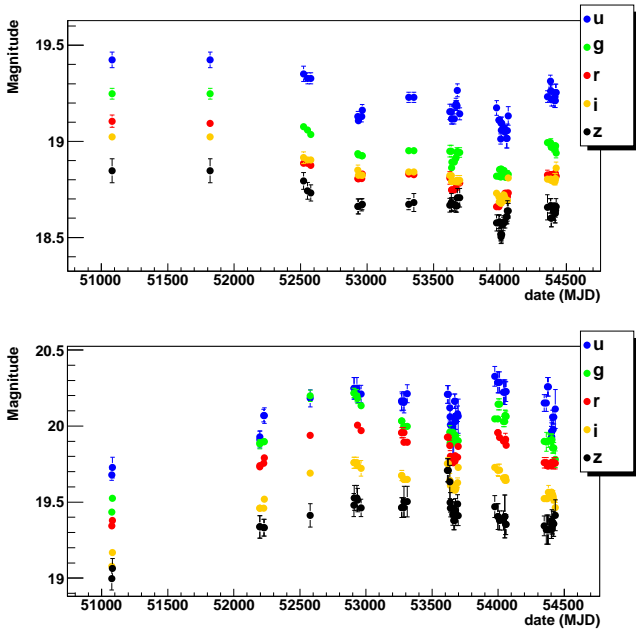


Fig. 3: Examples of light curves in the five SDSS photometric bands for quasars in Stripe 82.

2.2. Pre-treatment of the light curves

Photometric outliers could alter significantly the values of the variability parameters, to the point of washing out any relevant information. The raw light curves were therefore cleaned of deviant points (irrespective of their origin, whether technical or photometric) in a two-step procedure. A 3-point median filter was first applied to the quasar light curve in each of the five bands, followed by a clipping of all points that still deviated significantly from a fifth order polynomial fitted to the light curve. Note that to avoid re-

moving too many photometric epochs, the clipping threshold, initially set at 5σ , was iteratively increased until no more than 10% of the points were rejected.

2.3. Light curves χ^2

While most stars have constant flux, quasars usually exhibit flux variations. As shown by Sesar et. al. (2007), at least 90% of bright quasars are variable at the 0.03 mag level, and the variations in brightness are on the order of 10% on time scales of months to years (Vanden Berk et. al., 2004).

Each of the *ugriz* light curves were fit by a constant flux, and the resulting χ^2 recorded. While most stars have a reduced χ^2 near unity, as expected for non-variable objects, quasar light curves tend to be poorly fit by a constant, resulting in a large reduced χ^2 , as illustrated in Fig. 4 for the *r* band. The χ^2 thus helps to distinguish non-varying stars from varying point sources.

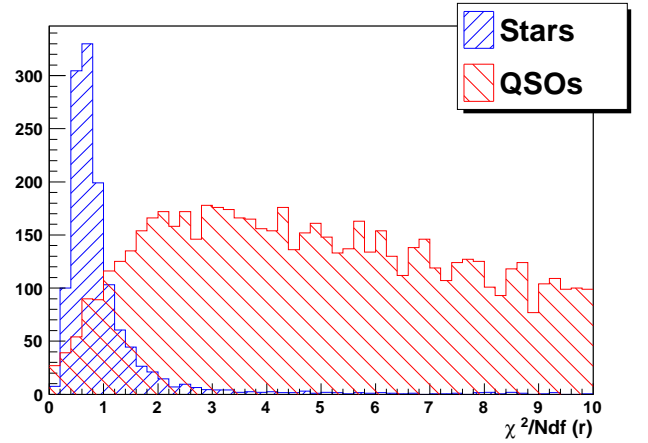


Fig. 4: Distribution of the reduced χ^2 resulting from the fit of light curves by a constant in the *r* band, for the stellar (blue) and the quasar (red) test samples. As confirmed by their larger reduced χ^2 , quasars clearly exhibit much larger deviations from a constant flux than stars.

2.4. Variability structure function

The structure function characterizes light curve variability by quantifying the change in amplitude Δm_{ij} as a function of time lag Δt_{ij} between observations at epochs i and j . Following the prescription of Schmidt et al. (2010), the variability structure function of the source magnitude, is given by

$$\mathcal{V}(\Delta t_{ij}) = |\Delta m_{i,j}| - \sqrt{\sigma_i^2 + \sigma_j^2}, \quad (1)$$

where σ is the magnitude measurement error. The structure function can be modeled by a power law $A(\Delta t)^\gamma$ in all photometric bands, illustrating the fact that, for quasars, the r.m.s. of the distribution of the magnitude difference between two observations tends to increase with time lag (cf. Fig. 5).

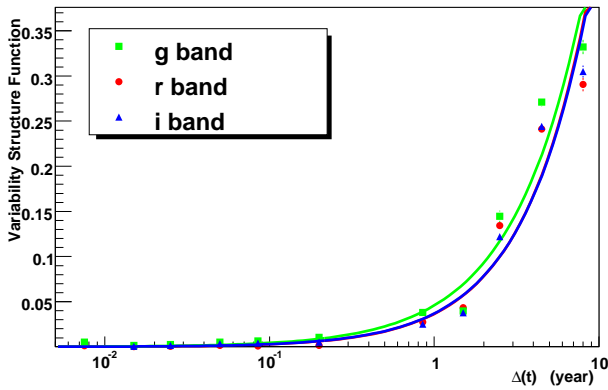


Fig. 5: Variability structure function $\mathcal{V}(\Delta t)$ of equation 1, for a typical quasar. The curves show the best-fit power law $A(\Delta t)^\gamma$ for the three bands g , r , i . Note that the r and i best-fits are almost identical.

To derive the power law parameters A and γ for a given light curve, we define the likelihood

$$\mathcal{L}(A, \gamma) = \prod_{j>i} \mathcal{L}_{ij}, \quad (2)$$

where for each ij pair of observations, an underlying Gaussian distribution of Δm values is assumed:

$$\mathcal{L}_{ij} = \frac{1}{\sqrt{2\pi\sigma(\Delta m)^2}} \exp\left(-\frac{\Delta m_{ij}^2}{2\sigma(\Delta m)^2}\right). \quad (3)$$

From the model above, the variability of the object, described by a power law, is naturally introduced in the definition of the variance $\sigma(\Delta m)^2$ of the underlying Gaussian distribution as

$$\sigma(\Delta m)^2 = [A(\Delta t_{ij})^\gamma]^2 + (\sigma_i^2 + \sigma_j^2). \quad (4)$$

The A and γ parameters were then obtained by maximization of the likelihood $\mathcal{L}(A, \gamma)$ with the MINUIT package.³

We found that for a given quasar, only the g , r and i bands had useful discriminating power, as quasars at high redshift have little flux in observed u -band, and because z -band light curves exhibit more noise than the other light curves. Furthermore, the fitted value of the γ parameter is roughly independent of the band. To reduce the uncertainty on the fitted parameters, we therefore chose to fit simultaneously the g , r and i bands for a common γ and three amplitudes (A_g , A_r , A_i). The range of values obtained for stars and quasars are shown in Fig. 6. Non variable objects (mostly stars) lie near the origin of the graph, while quasars populate the region of larger A and γ values. It is interesting to notice that this approach can also distinguish various variable populations. RR-Lyrae, for instance, can have large variations (thus large A) but with no (or little) trend in time, implying that γ remains small.

2.5. Variability selection of quasars using a Neural Network

To complete our method for discriminating stars from quasars, an artificial Neural Network (NN) was

³ <http://wwwasdoc.web.cern.ch/wwwasdoc/minuit/min-main.html>

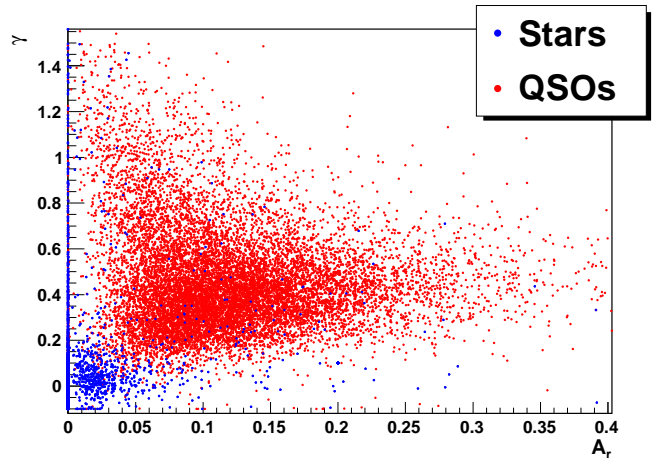


Fig. 6: Parameters γ and A_r of the variability structure function for the stellar (blue points) and quasar (red points) test samples. Large A 's indicate large fluctuation amplitudes. Large γ 's indicate an increase of the fluctuation amplitude with time.

used (Bishop, 1995).⁴ The basic building block of the NN architecture is a processing element called a neuron. The NN architecture used in this study is illustrated in Fig. 7, where each neuron is placed on one of four “layers”, with N_l neurons in layer l .

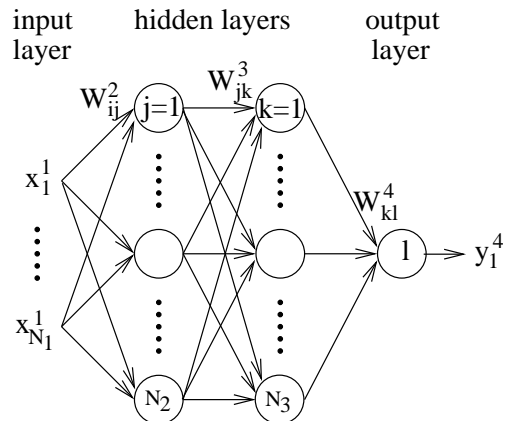


Fig. 7: Schematic representation of the artificial neural network used here with N_1 input variables, two hidden layers, and one output neuron.

The output of each neuron on the first (input) layer is one of the N_1 variables defining an object. For the present study, $N_1 = 9$ (five χ^2 's and four structure function parameters γ , A_g , A_r and A_i). The inputs of neurons on subsequent layers ($l = 2, 3, 4$) are the N_{l-1} outputs (the x_j^{l-1} , $j = 1, \dots, N_{l-1}$) of the previous layer. The inputs of any neuron are linearly combined according to “weights” w_{ij}^l and “offsets” θ_j^l :

$$y_j^l = \sum_{i=1}^{N_{l-1}} w_{ij}^l x_i^{l-1} + \theta_j^l \quad l \geq 2. \quad (5)$$

⁴ We used a C++ package, TMultiLayerPerceptron, developed in the ROOT environment (Brun et al., 1995).

The output of neuron j on layer l is then defined by the non-linear function

$$x_j^l = \frac{1}{1 + \exp(-y_j^l)} \quad 2 \leq l \leq 3. \quad (6)$$

The fourth layer has only one neuron giving an output $y_{\text{NN}} \equiv y_1^4$, with $0 \leq y_{\text{NN}} \leq 1$, reflecting the likelihood that the object defined by the N_1 input variables is a quasar.

Certain aspects of the NN procedure, especially the number of layers and the number of nodes per layer, are somewhat arbitrary. They are chosen by experience and for simplicity. In contrast, the weights and offsets must be optimized so that the NN output, y_{NN} , correctly reflects the probability that an input object is a quasar. To determine the weights and offsets, the NN must therefore be “trained” with a set of objects that are spectroscopically known to be either quasars or stars (e.g. the test samples described in Sec. 2.1).

The result of the NN output is illustrated in Fig. 8. As expected, stars peak near 0 while quasars have an output value near 1, and very few objects appear in the middle range where the classification is uncertain.

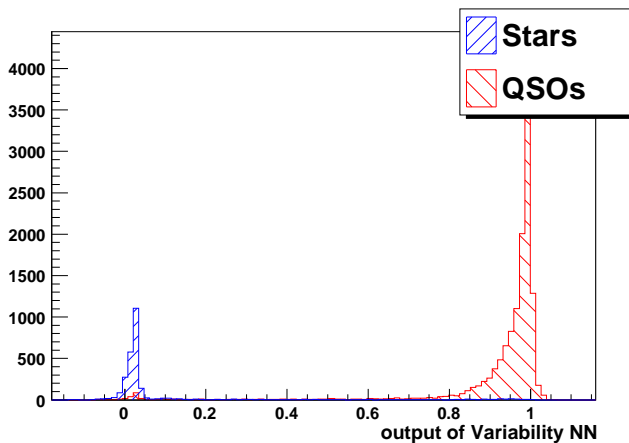


Fig. 8: Output of the variability Neural Network for the star and quasar samples. 97% of the quasars have $y_{\text{NN}} > 0.5$, and 3% are classified as stellar-like ($y_{\text{NN}} < 0.5$).

For this study, we concentrated on objects with at least 4 observation epochs. In Stripe 82, 13063 spectroscopically confirmed quasars met this requirement. Of these, 383 only (3%) are not classified as “quasar-like” by the variability NN, i.e. yield a NN output smaller than 0.5. A visual inspection of their light curves confirms that they exhibit no clear variability, neither on short nor on long time-scales. A minimum loss of $\sim 3\%$ is therefore to be expected for any variability-based algorithm to select quasars using these data. This loss approaches 5% for the subsample of 3571 quasars at $z > 2.15$, probably due to the lower photometric precision of the objects. Part of the loss might also be due to the smaller rest frame time gap at increasing redshift.

To quantify the performance of our quasar selection, we define the completeness C and the purity P :

$$C = \frac{\text{Number of selected quasars}}{\text{Total number of confirmed quasars}}, \quad (7)$$

$$P = \frac{\text{Number of selected quasars}}{\text{Total number of selected objects}}. \quad (8)$$

We also define the stellar rejection R as

$$R = 1 - \frac{\text{Number of selected stars}}{\text{Total number of stars in the sample}}. \quad (9)$$

Fig. 9 illustrates the performance, in terms of quasar completeness and stellar rejection, of the variability-based NN, for the two subsets of low- z and high- z quasars of the test sample. It is noteworthy that the latter class is only 2 to 5% less complete than the low redshift sample (for an identical stellar rejection).

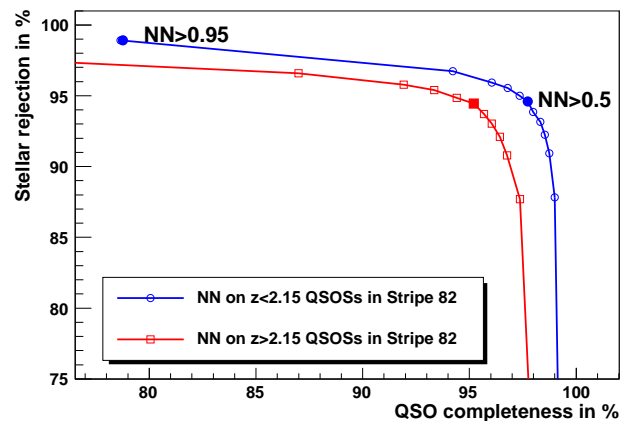


Fig. 9: Stellar rejection R vs. quasar completeness for the variability-based NN. Open circles are for known low-redshift quasars, squares for those with $z > 2.15$. Filled symbols at $R \sim 94.5\%$ and $R \sim 98\%$ indicate the location of these curves of the selection thresholds used in Sec. 3.1 and 3.2.

The small redshift-dependence of the variability-based selection method is further confirmed in Fig. 10, which shows $C(z)$ for the two thresholds on the output of the variability NN used in Sections 3.1 and 3.2. In contrast to a standard quasar selection based on colors, the completeness obtained here depends smoothly on redshift and has no minimum at any particular redshift. For a loose cut on the output of the variability NN ($\text{NN}_{\text{var}} > 0.50$), a high completeness is achieved at all redshifts. As the cut is tightened ($\text{NN}_{\text{var}} > 0.95$), however, a strong decrease with redshift appears, due to the reduced elapsed rest-frame time at high redshift, and to the decrease in the light curve signal-to-noise ratio as objects become fainter, resulting in a weaker significance of the variability. Nevertheless, even with a tight cut, the method still does not introduce any sharp redshift-specific feature.

The purity of the selection cannot be determined as easily since it strongly depends on the reference sample. Furthermore, not all existing quasars, even in the redshift range of interest, have yet been identified. Objects selected through their variability might thus be confirmed as being quasars although they were not selected by previous color selections. Purity will therefore be given in Sec. 3.3, for two cases where the variability selection has been applied to actual data.

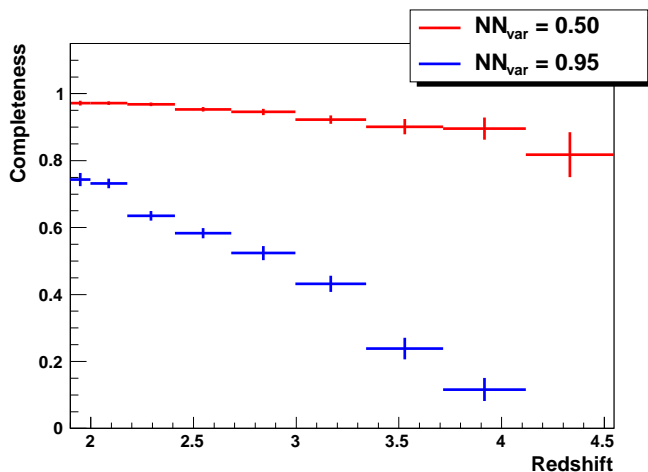


Fig. 10: Completeness C vs. redshift for two thresholds on the output of the variability NN corresponding to those used for the selections of Sec. 3.1 (main sample, with $NN_{\text{var}} > 0.50$) and 3.2 (extreme variability sample, with $NN_{\text{var}} > 0.95$).

3. Variability-based selection for BOSS

BOSS is aiming for a density of $\sim 20 \text{ deg}^{-2}$ quasars at redshifts $z > 2.15$ (hereafter called “high- z ” quasars), with an allocation of 40 deg^{-2} optical fibers to obtain spectra of quasar candidates. In this context, the above study can be applied with two major goals.

The first one is to improve the purity of the list of quasar candidates for which the spectra will be obtained. In BOSS, a traditional color-based selection based on single epoch photometry typically reaches a quasar density of $10\text{--}15 \text{ deg}^{-2}$ from an initial selection of $\sim 40 \text{ deg}^{-2}$ targets. An algorithm with a higher purity presents the advantage of reaching the desired quasar density for BOSS while keeping the number of fibers fixed. This is the aim of the “Main sample” described in Sec 3.1.

The second goal is to search for additional possible quasars, that would have been missed by previous searches because of unusual colors, but that could be selected based on their variability. This is the strategy leading to the selection of the “Extreme variability sample” presented in Sec. 3.2.

Both approaches were adopted by BOSS for the observation of Stripe 82 in September and October 2010. The results obtained are given in Sec. 3.3, and a comparison with a color-based selection from co-added photometry is described in Sec. 3.4.

3.1. Main sample

The goal of the Main sample was to obtain a list of 31 deg^{-2} targets with high quasar purity, the remaining 9 deg^{-2} being kept for other selections or lost at the tiling stage (Blanton et al., 2003).

A color-based analysis on ~ 20 co-added observations (cf. Fig. 11) with very loose thresholds is used to yield an initial list of $\sim 70 \text{ deg}^{-2}$ objects, expected to be dominated by stars by at least a ratio 2:1. The criteria for this preselection were:

- output of a color-based NN > 0.2 (with colors determined from co-added observations) to remove objects that were *not* in the vicinity of the quasar locus in color-space (Yeche et al., 2010),
- $(u - g) > 0.15$ to enhance the fraction of $z > 2.15$ quasars over low- z ones. This cut rejects only 1% of previously known high- z quasars.

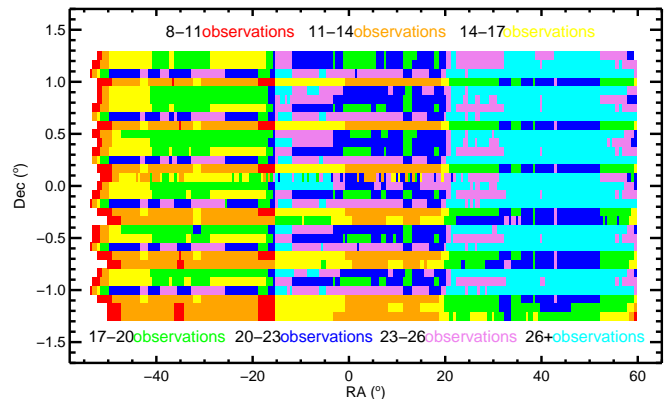


Fig. 11: Number of SDSS-I and SDSS-II measurements used to derive the co-added photometry in Stripe 82.

The completeness of this preselection for high- z quasars is of order 85%, which corresponds to an upper bound on the completeness of the “main sample”.

Requiring the output on the variability NN to be larger than 0.50 (and removing previously identified low redshift quasars) yielded a selection of 35 deg^{-2} objects, which is reduced to 31 deg^{-2} for technical reasons related to the tiling of the objects. As shown in Fig. 10, the completeness of the variability selection at this threshold is expected to be $\sim 95\%$ (of the sample to which it is applied).

Fig. 12 shows that the target density is flat with Right Ascension, as expected for extragalactic objects, in contrast to the peaks that would be expected for $\alpha_{J2000} \simeq -43^\circ$ in the case of large contamination by Galactic stars as is seen in the initial distribution corresponding to a loose photometric selection.

3.2. Extreme variability sample

The second goal was to obtain an independent and complementary list of about 3 deg^{-2} objects selected by the variability NN but rejected according to their colors. With this approach, we could expect to find quasars in the stellar locus, at the risk of obtaining a sample dominated by variable stars rather than by quasars.

The total number of point-like objects in Stripe 82 is on the order of several millions. Because the computation of the variability parameters on such a large sample would have been both disk- and time-consuming, a very loose preselection of about 1000 deg^{-2} objects was first applied, with the following criteria:

- $i > 18$ to limit the contribution from low- z quasars but $g < 22.3$ to maintain the possibility to obtain a good spectrum,

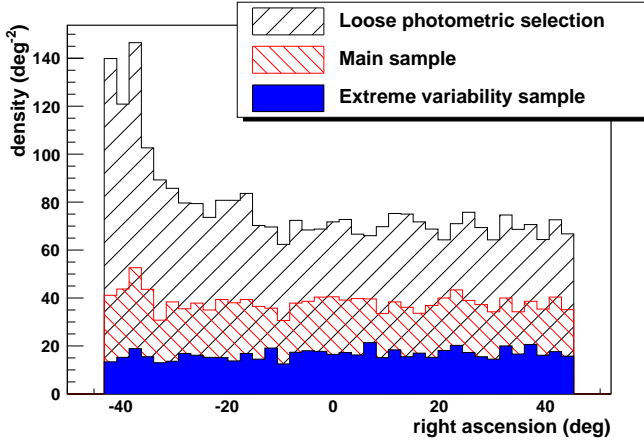


Fig. 12: Right Ascension distribution of targets in the main sample at the stage of loose color-based selection (black histogram), and after the final variability-based selection (red histogram). The targets of the extreme variability program are shown as the blue histogram.

- $(g - i) < 2.2$ to exclude M stars,
- $(u - g) > 0.4$ to enhance the fraction of $z > 2.15$ quasars compared to low- z ones,
- $c_1 < 1.5$ or $c_3 < 0$ to remove a region in color-space distant from quasars and strongly populated by stars, where colors c_1 and c_3 are defined in Fan (1999) as

$$c_1 = 0.95(u - g) + 0.31(g - r) + 0.11(r - i),$$

$$c_3 = -0.39(u - g) + 0.79(g - r) + 0.47(r - i).$$

While these cuts reduced the total number of objects by about a factor of ten, they rejected only about 5% of previously known quasars.

Requiring the output of the variability NN to be greater than 0.95 (i.e. selecting the most variable objects) and removing all objects already present in the main sample, yielded a selection of $\sim 3 \text{ deg}^{-2}$ objects, as planned. The distribution of the Right Ascension of the selected objects is shown in Fig. 12 as the blue histogram. Its flatness is again an indication of low stellar contamination.

3.3. Results

The reduction of the spectra were performed by the BOSS pipeline (Bolton & Schlegel, 2009), which also gives a preliminary determination of the redshift of the identified quasars. All spectra were checked visually to yield final identifications and redshifts. The pipeline and visual scanning are in agreement for $\sim 95\%$ of the objects.

The outcome of the targeting of the two samples described above is summarized in Table 1. A significant improvement over previous results is apparent. Only $\sim 4 \text{ deg}^{-2}$ targets out of 35 are not quasars, which is in agreement with the flat Right Ascension distributions of Fig. 12.

The main sample has a quasar purity of 93% on average and 72% at a redshift $z > 2.15$. From this sample alone, the average density of $z > 2.15$ quasars over Stripe 82 has been increased from $\sim 15 \text{ deg}^{-2}$ from previous BOSS observations to 22.3 deg^{-2} .

It is remarkable that 86% of the objects in the “Extreme var. only” category, all rejected according to their colors, are quasars. Furthermore, half of these are at $z > 2.15$.

Considering the full sample selected from its extreme variability (including the candidates in the main sample that fulfilled the requirement $\text{NN}_{\text{var}} > 0.95$, cf. line “Extreme var.” of Table 1), we achieve an even higher purity: 96% of the objects are quasars, and 80% are at a redshift above 2.15. These results imply that variability is indeed an efficient tool for selecting quasars against all other variable sources.

The low fiber budget allocated to the Extreme variability program does not make the study of its completeness a relevant issue. However, we note that with a target density of only 3 deg^{-2} , the extreme variability program raised the high- z completeness of the main sample by $\sim 6\%$.

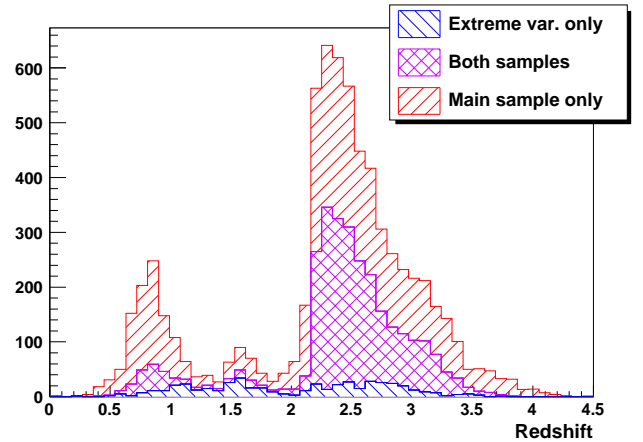


Fig. 13: Stacked redshift distribution of the confirmed quasars, where the histograms represent the number of quasars in each of the non-overlapping samples. The total extreme-variability sample is thus illustrated by the blue+purple surface, while the total main sample is in purple+red. The emphasis of the selection on $z > 2.15$ objects is apparent.

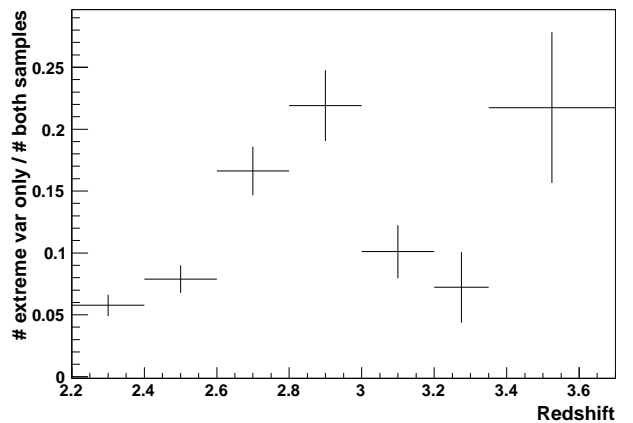


Fig. 14: Redshift distribution of the fraction of quasars added by the extreme variability selection compared to quasars in the same variability range but fulfilling color constraints.

Fig. 13 shows the redshift distribution of the quasar samples selected through variability. As expected, after ap-

Selection sample	Target density	All quasar		$z > 2.15$ quasar		
		Density	$P(\%)$	Density	$P(\%)$	$C(\%)$
Main sample	31.1	29.0	93	22.3	72	84
Extreme var.	15.1	14.6	96	12.1	80	45
Extreme var. only	3.4	2.9	86	1.7	49	-
Total	34.5	31.9	92	24.0	69	90

Table 1: Density, purity P and completeness C of variability-based selections of quasar candidates. All densities are in deg^{-2} . The purity is the ratio of the density of the quasars in a given sample to the target density. The completeness includes all identified high-redshift quasars, whether from their color, variability, radio emission etc. The “Target” column is for all candidates, “All quasar” refers to confirmed quasars independently of their redshift, “ $z > 2.15$ ” to the subset of high-redshift quasars. The line “Extreme var. only” refers to objects that were rejected as quasars (e.g. from the main sample) due to their colors. The line “Extreme var.” includes both the extreme variability sample and the targets in the main sample that fulfilled the requirement $\text{NN}_{\text{var}} > 0.95$. As stated in the abstract, we see that 90% of the known high-redshift quasar population is recovered by its variability, and that 92% of the selected targets are quasars (i.e., only 8% non-quasars).

plying the cut on $u - g$, most are at $z > 2.15$, corresponding to the requirements of BOSS. Fig. 14 shows that the additional quasars selected via extreme variability tend to preferentially lie in the $2.5 < z < 3.0$ redshift range where color-based selections are known to be incomplete. This indicates that a pure variability-based selection can indeed contribute to the recovery of quasars lost during the color-color selection. The low number of quasars at $z > 3.4$ prevents firm conclusions from being drawn on this higher redshift range.

The location of the additional quasars in color-color space is given in Fig. 15. There is no indication that they form a new class of quasars; instead, they appear to extend the quasar locus into the stellar locus, as expected from synthetic models of quasar evolution (Fan, 1999).

The fraction of Broad Absorption Line (BAL) quasars among the $z > 2.15$ quasars is seen to be higher in the sample selected through its variability than in the main sample that includes some color cuts. Comparing the two non-overlapping “main” and “extreme var only” samples, we have

$$\frac{\text{Number of high } z \text{ BAL quasars}}{\text{Number of high } z \text{ quasars}} = \begin{array}{l} 7.0\% \pm 0.4\% \quad (\text{Main sample}) \\ 14.6\% \pm 1.8\% \quad (\text{Extreme var. only}) \end{array}$$

This seems to indicate that quasars affected by BAL features tend to fall outside the color regions that are generally favored by quasars.

3.4. Comparison with color selection on co-added photometry

The large number of observations in Stripe 82 also permits a color-based selection of quasars using photometry obtained on co-added images, i.e. deeper frames and with a higher signal-to-noise. We used this photometry to derive a list of 35 deg^{-2} targets, already expected to be much more complete than the traditional list based on single epoch observations. We compared the outcome of this improved selection to that of the variability-based one (“Main” and “Extreme variability” samples) described in the paper. Variability yields a number of recovered quasars that is 20% to 30% higher than the color selection, the result depending slightly on the method used (likelihood, neural network... or a combination of these). The excess might have been larger still with a larger ratio of the 35 deg^{-2} fibers allocated to the

extreme-variability sample, since the latter has a higher purity than the main sample (cf. Tab. 1). As variability and colors seem to yield complementary samples (some quasars can be selected one way and not in the other), the most promising method would be to use both pieces of information simultaneously.

4. Application to the full SDSS sky

Given the success of the variability-based selection in Stripe 82, it would be interesting to apply it over a much wider area in the sky. One possibility would be to use jointly data from SDSS (one or two photometric measurements over $10,000 \text{ deg}^2$) and forthcoming data from the Palomar Transient Factory (PTF) or Pan-STARRS 1 (PS1), which cover the same $10,000 \text{ deg}^2$ at several occasions over 3 to 5 years. A strategy based on these various data sets can be useful to future surveys like BigBOSS⁵ or LSST (LSST, 2009; Ivezić et al., 2008).

4.1. Extrapolation to PTF

Since December 2008, PTF has taken data in the R band at the cadence of one measurement every 5 nights (Rau et al., 2009). The images can be co-added to produce 4 deep frames per year of observation. Apart from Stripe 82, most of the area covered by SDSS has been observed only once. The data available for quasar searches at the end of the PTF survey can therefore be expected to consist typically of 1 point from SDSS (useful to extend the lever arm in time lag) and 4 points per year from PTF. To explore the possibilities offered by this data combination for quasar selection, we constructed synthetic light curves by down-sampling data from Stripe 82 in the following way:

- The last 5 years of SDSS are used to simulate PTF measurements: four evenly spaced points per year are selected from the SDSS data,
- To simulate the sole measurement available from SDSS on most of the sky, one point is taken at random over the previous years of SDSS, maintaining a gap of at least 2 years between the SDSS point and the first PTF measurement (to ensure a realistic lever arm).

Only synthetic light curves with all 21 measurements (1 for SDSS and 4 for each of the 5 years of PTF) are considered hereafter. With this constraint, we are left with 2248

⁵ <http://bigboss.lbl.gov>

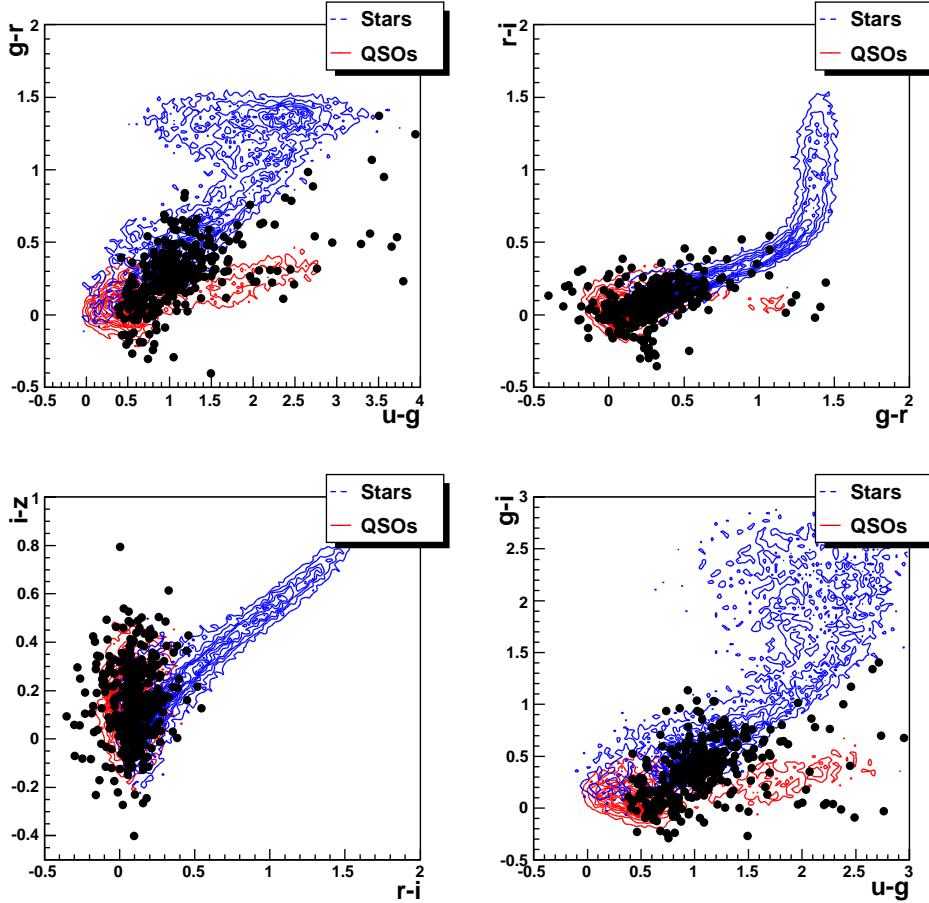


Fig. 15: Color-color plots indicating the stellar (blue) and quasar (red) loci, as well as the position of the 370 high-redshift additional quasars rejected from their colors but selected through the variability neural network (extreme variability sample described in Sec. 3.2).

(83%) stellar and 11456 (86%) quasar light curves (out of the initial samples described in section 2.1).

As PTF observes only in one band, the variability parameters are reduced to the reduced χ^2 in r , A_r and γ . A neural network was trained on the usual stellar and quasar test samples to yield an estimator of quasar likelihood based on these 3 parameters. The red triangles in Fig. 16 mark the evolution of the stellar rejection vs. quasar completeness as the threshold on the NN output is varied. They show that one can reach a quasar completeness of 85% for a rejection of 91% of the stars. For comparison, the blue dots illustrate the favorable case of Stripe 82 with all available measurements on 5 bands (case studied in Section 3) and a variability selection based on the 9-parameter NN.

Note that the stellar sample used for figure 16 has passed loose color cuts that might not be available for PTF data. We have checked that the performance of the algorithm in the rejection of randomly picked Stripe 82 objects, statistically dominated by stars by at least a ratio 10 to 1, is within 1% of the performance plotted in the figure.

4.2. Extrapolation to PS1

Pan-STARRS 1 (PS1) started regular observations in March 2009. With its 3 degree field of view, the whole available sky is recorded 3 times during the dark time of each lunar cycle. The first part of the project is expected to last about 3 years, after which a second telescope will begin operation. To explore the use of the PS1 data, we proceeded in a similar way as for PTF. The main difference is that PS1 has data available in five filters (g , r , i , z and y) instead of one. For quasar selection in the redshift range $2.15 < z < 4$, we considered only the filters in common with SDSS (g through z). This restriction produced 8 variability parameters: four χ^2 's (one in each of the four bands), A_g , A_r , A_i and the common γ (as for the study of Stripe 82). As for PTF, a NN was trained to yield an estimator based on these 8 parameters. The performance of the resulting selection is illustrated in Fig. 16 for two survey durations, 3 or 5 years. Only synthetic light curves with all 13 (in the case of a 3-year survey) or 21 (in the case of a 5-year survey) measurements are considered in the plot.

The 3-year survey gives results comparable to those for the 5-year PTF. In contrast, the 5-year PS1 survey is a significant improvement over the 3-year survey, and can reach

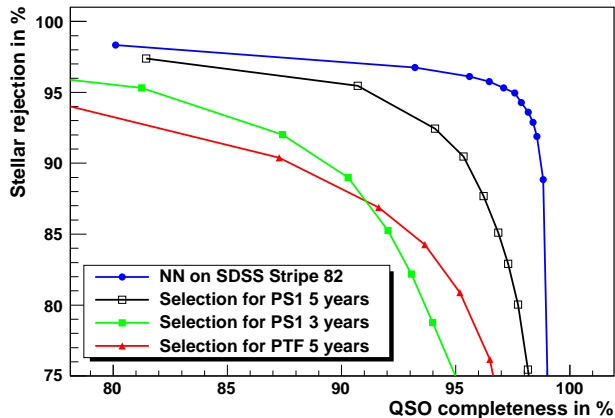


Fig. 16: Stellar rejection vs. quasar completeness for the full Stripe 82 data (blue dots), for the Pan-STARRS (green and black squares) and for the PTF (red triangles) simulated data. In each case, the threshold on the relevant variability NN is increased from right to left.

an 85% quasar completeness for a 97% stellar rejection, or a 91% quasar completeness for a 95% stellar rejection.

The absence of the SDSS anchor point would reduce the quasar completeness by about 3%. Of course, the SDSS data would have little impact on the stellar rejection R , since most stars exhibit flat light curves, whatever their coverage.

In this work, the cut-off for quasar selection was set at $g < 22.3$. Future surveys like BigBOSS intend to go deeper in order to increase the density of quasars. To study the impact of the value of this limit on the performance of the variability selection, we computed stellar rejection vs. quasar completeness for $g < 21$, $g < 22$ and $g < 23$, in the case of five years of PS1 data. The quasar sample is the same as before, but the stellar sample is taken to be a set of random objects in a 7.5 deg^2 region in Stripe 82 around $\alpha_{J2000} = 0$. The stellar sample contains ~ 1000 objects per deg^2 at $g < 21$ and ~ 2500 objects per deg^2 at $g < 23$. Fig. 17 shows that the stellar rejection decreases only by $\sim 2\%$ (at a 95% quasar completeness) when changing the limit from $g < 22$ to $g < 23$. The major impact of lowering the limit is therefore an increase in the number of selected stars that follows the increase in stellar density with the inclusion of fainter objects.

Although the variability method cannot lead to results as good for the sparser data of Pan-STARRS (13 to 21 measurements in four bands) or PTF (21 measurements in one band) as for the SDSS data on Stripe 82 (~ 50 measurements in five bands), it can still contribute significantly to quasar selection. Used in addition to a color selection, as was done with BOSS for Stripe 82, even from a single epoch in SDSS (for areas other than Stripe 82), it can result in much improved selections than what color-selection alone can achieve.

5. Conclusions

We have designed a method that characterizes light curve variability in order to discriminate quasars from both non-variable and variable stars. A Neural Network was imple-

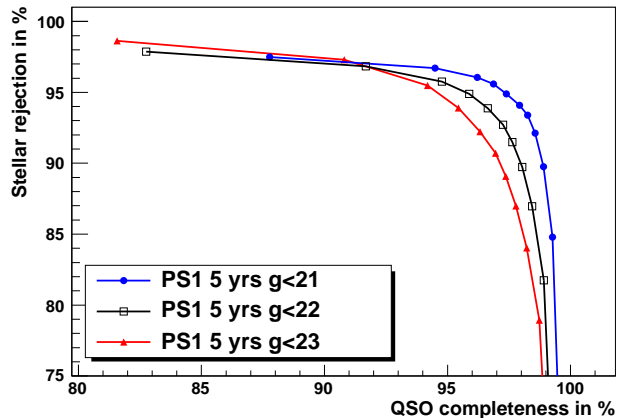


Fig. 17: Stellar rejection vs. quasar completeness for five years of Pan-STARRS simulated data. The depth of the stellar sample varies from $g < 21$ (blue) to $g < 23$ (red curve). The points are affected by a systematic uncertainty on the stellar rejection of order 1% due to the uncertainty on the estimated number of quasars that we remove from the “stellar” (e.g. random object) sample.

mented to yield an estimator of quasar likelihood derived from these variability parameters.

The method has been applied in conjunction with a loose color-based preselection to define a list of 31 deg^{-2} targets in Stripe 82 for which spectra were taken with BOSS. The performance of this selection on quasars at redshift above 2.15 can be quantified by a purity of 72% and a completeness of 84%. This represents a significant improvement over traditional fully color-based selections which seldom obtained a purity in excess of 40%.

A second study was dedicated to the objects exhibiting an extreme quasar-like variability. An additional 3 deg^{-2} targets were selected on the following criteria: the objects had to be excluded from the previous sample (i.e. did not have favorable colors according to quasar standards), and had a very high value of the output of the variability NN. Half of the objects thus selected proved to be high redshift quasars, 40% low redshift quasars and only 10% were uncertain or stars. This program thus increased further the completeness of the quasar selection, reaching the unprecedented value of 90% total on average over Stripe 82.

Combining the above two programs allowed BOSS to obtain a density of $z > 2.15$ quasars in Stripe 82, all selected through their variability, of 24.0 deg^{-2} , with only $\sim 35 \text{ deg}^{-2}$ fibers dedicated to their identification.

The method developed here was also applied to ersatz data from Palomar Transient Factory or from Pan-STARRS to determine the performance that can be achieved for future target selections of quasars over about $10,000 \text{ deg}^{-2}$ of the sky.

Acknowledgements. Funding for SDSS-III has been provided by the Alfred P. Sloan Foundation, the Participating Institutions, the National Science Foundation, and the U.S. Department of Energy. The SDSS-III web site is <http://www.sdss3.org/>.

SDSS-III is managed by the Astrophysical Research Consortium for the Participating Institutions of the SDSS-III Collaboration including the University of Arizona, the Brazilian Participation Group, Brookhaven National Laboratory, University of Cambridge, University of Florida, the French Participation Group, the German

Participation Group, the Instituto de Astrofísica de Canarias, the Michigan State/Notre Dame/JINA Participation Group, Johns Hopkins University, Lawrence Berkeley National Laboratory, Max Planck Institute for Astrophysics, New Mexico State University, New York University, the Ohio State University, the Penn State University, University of Portsmouth, Princeton University, University of Tokyo, the University of Utah, Vanderbilt University, University of Virginia, University of Washington, and Yale University.

ES is supported by grant DE-AC02-98CH10886. The BOSS French Participation Group is supported by Agence Nationale de la Recherche under grant ANR-08-BLAN-0222.

References

- Abazajian K. et al., 2009, *ApJS*, 182, 543
Adelman-McCarthy J.K. et al., 2008, *ApJS*, 175, 297
Bishop, C. M., “Neural Networks for pattern recognition”, 1995, Oxford University Press
Blanton, M.R., et al., 2003, *AJ*, 125, 2276
Bolton, A.S. and Schlegel, D.J., 2010, *PASP*, 122, 248
+ BOSS pipeline
Brandon, K.C., Bechtold, J. and Siemiginowska, A, *AJ*, 2009, 698, 895
Butler, N. and Bloom, J., 2010, arXiv:1008.3143
Brun, R. et al. (the ROOT Team), <http://root.cern.ch>
Cole, S. et al., (the 2dFGRS Team), 2005, *MNRAS*, 362, 505
Croom, S.M. et al., 2001, *MNRAS*, 322, 29
Croom, S. M. et al., 2004, *MNRAS*, 349, 1397
Croom, S. M. et al., 2009, *MNRAS*, 392, 19
de Vries, A., et al., 2004, *AJ*, 129, 615
Dobrzycki, A., Macri, L., Stanek, K. and Groot, P., 2003, *AJ*, 125, 1330
Eisenstein D. J. et al., (the SDSS Collaboration), 2005, *ApJ*, 633, 560
Fan, X., 1999, *AJ*, 117, 2528
Frieman, J. et al., 2008, *AJ*, 135, 338
Fukugita, M., Ichikawa, T., Gunn, J.E., Doi, M., Shimasaku, K., and Schneider, D.P. 1996, *AJ*, 111, 1748
Geha, M. et al., 2003, *AJ*, 125, 1
Gunn, J.E., et al. 1998, *AJ*, 116, 3040
Gunn, J.E., et al. 2006, *AJ*, 131, 2332
Ivezic Z., Tyson J. A., Allsman, R. et al. (LSST Collaboration), arXiv:0805.2366
Kozłowski, S. et al., *AJ*, 2010, 708, 927
LSST Science coll., 2009, version 2.0, arXiv:0912.0201
MacLeod, C.L. et al., 2008, arXiv:0810.5159
MacLeod, C.L. et al., 2010a, *ApJ*, 721, 1014
MacLeod, C.L. et al., 2010b, arXiv:1009.2081
McDonald, P. & Eisenstein, D., 2007, *Phys. Rev. D.*, 76, 063009
Nugent, P., private communication
Percival, W. et al., 2010, *MNRAS*, 401, 2148
Rau, A. et al., 2009, *PASP*, 121, 886
Rengstorf, A. et al., 2004, *ApJ*, 606, 741
Richards, G.T. et al., 2004, *AJS*, 155, 257
Richards, G.T. et al., 2006, *AJ*, 131, 2766
Richards, G.T. et al., 2009, *AJS*, 180, 67
Schneider, D.P. et al., 2010, *AJ*, 139, 2360
Schlegel, D., White, M., and Eisenstein, D., 2009, arXiv:0902.4680
Schmidt, M. and Green, R.F., 1983, *ApJ*, 269, 352
Schmidt, K.B. et al., 2010, *ApJ*, 714, 1194
Sesar, B. et al., 2007, *AJ*, 134, 2236
Stoughton C. et al., 2002, *AJ*, 123, 485
Vanden Berk, D. et al., 2004, *ApJ*, 601, 692
White, M., 2003, arXiv:0305474
Worseck G. and Prochaska J.X., 2010, arXiv:1004.3347
Yeche, Ch. et al., 2010, to appear in *A&A* (arXiv:0910.3770)
York, D.G., et al. 2000, *AJ*, 120, 1579